http://dx.doi.org/10.11142/jicems.2012.1.4.517
Journal of International Conference on Electrical Machines and Systems vol. 1, no. 4, pp. 517~524, 2012 517

Modeling and Evaluation of Linear Oscillating Actuators

X. Chen* and Z. Q. Zhu*

Abstract – The operation of linear oscillating system is complicated, involving system nonlinearities of both actuator and load, and variations of driving frequency in order to track the mechanical resonance. In this paper, both analytical and state-variable modeling techniques are used to investigate the influence of actuator parameters, such as back-emf/thrust force coefficient and cogging force, on the performance of linear oscillating systems. Analytical derivations are validated by simulations, and good agreements are achieved. The findings of the paper can greatly facilitate the design and evaluation processes of permanent magnet linear actuators.

Keywords: **Linear actuator, Permanent magnet, State-variable modeling**

1. Introduction

The operation of linear oscillating system is relatively complicated, usually involving system nonlinearities of both actuator and load, and variations of driving frequency in order to track the mechanical resonance. Hence, the state-variable modeling technique in the time domain is extensively employed to study the dynamic and steady state characteristics of linear oscillating systems. Depending on the linearity of the specific system, such as the load force vs. displacement, spring stiffness vs. displacement, actuator thrust force vs. displacement and actuator thrust force vs. supply current etc, either the linear or nonlinear state-variable modeling can be used. For simple analysis and control or cases where no severe nonlinearity is observed, the linear state-variable modeling can be readily adopted, for example in [1] and [2]. However, if nonlinearity is too significant to be neglected, the nonlinear state-variable modeling has to be used. By way of example, both [3] and [4] store the nonlinear finite element (FE) predicted actuator performance in terms of cogging force, force coefficient, inductance, etc as look-up tables, whilst the gas force characteristic of linear compressors can be modeled by an ideal pneumatic model, [5], [6]. Additionally, transient FE analyses can be incorporated into the simulation process, as done in [7] and [8]. Although it is very time-consuming, this is conducive to obtain a more accurate simulation compared to the real behavior of the oscillating system.

Despite that there are many publications available discussing the state-variable modeling of linear oscillating systems, very few have studied the inherent influence caused by the nonlinear performance of linear oscillating actuators. Therefore, in this paper the influence of actuator performance, such as back-emf/thrust force coefficient and cogging forces, on oscillating systems are investigated analytically with particular reference to permanent magnet (PM) linear oscillating actuators (LOA). Then, simulations in MATLAB/Simulink are undertaken to validate the foregoing analytical models.

2. State-variable Modeling of Linear Oscillating Systems

Generally, the linear oscillating system can be divided into 2 coupled sub-systems, viz. the electromagnetic and mechanical systems. The electromagnetic system converts the electrical energy to mechanical energy via the magnetic fields in the LOA, the developed electromagnetic force being dependant on the supply current and the displacement of moving parts. Neglecting the cross-coupling effect and assuming linear magnetic circuits, the electromagnetic system of a 1-phase PM oscillating system can be modeled by the governing voltage equation formulated as:

$$u = Ri + L\frac{di}{dt} + iv\frac{dL}{dx} + v\frac{d\psi_m}{dx} \tag{1}$$

where u and i are the voltage and current of power supply; R and L are the winding resistance and self-inductance; Ψ

* Dept. of Electronic and Electrical Engineering, the University of Sheffield, UK (carnchen@hotmail.com, Z.Q.Zhu@sheffield.ac.uk)
Received 13 October 2012; Accepted 10 November 2012

and Ψ_m are the total winding flux-linkage and the flux-linkage due to PM; x and v are the displacement and velocity of the moving parts. Based on (1), it can be seen that the reluctance force (F_R) and excitation force (F_E) are given by (2a) and (2b), whilst the total thrust force (F_{act}) produced by LOA is defined as (2c).

$$F_R = \frac{1}{2} i^2 \frac{dL}{dx} \tag{2a}$$

$$F_E = i \frac{d\psi_m}{dx} = K_E i \tag{2b}$$

$$F_{act} = F_C + F_R + F_E \tag{2c}$$

where K_E, namely the back-emf/force coefficient, is the derivative of the winding flux-linkage due to PM over the displacement, while the equation of cogging force (F_C) not given due to its complex nature.

Secondly, the mechanical state-variable equation, (3), can be employed to predict the mechanical behavior of linear oscillating systems.

$$F_{act} - F_L - K_s x - D_e v = m_e \frac{d^2 x}{dt^2} \tag{3}$$

where F_L is the load force; m_e is the effective moving mass; K_s is the effective stiffness of the mechanical spring; D_e is the effective viscous damping coefficient of the oscillating system mainly due to the hysteresis loss of the spring and the bearing friction. As for the load force, there are several different fixtures available, typically the frictional load, linear generator load, linear compressor load, etc. However, the fundamental approach for the modeling of different load forces is identical, i.e. to convert the load forces into equivalent stiffness and damping components and substitute it with them in (3).

It should be noted that although it is clearly the most straightforward and cost-effective way to drive linear oscillating systems by sinusoidal or rectangular voltage supplies, this is incapable of fully characterizing the system, because it ultimately relies on the induced current to determine the actuator performance. Whereas the current control method is equally applicable to linear oscillating systems, just as in rotary machines. Under the sinusoidal current control, the benefit of higher efficiency is observed in [9], whilst [6] finds that the instable jump problem of the oscillating amplitude, [10], is effectively eliminated. Therefore, the current control method will be used in this paper by commanding the supply current to be:

$$i = I_0 \sin(\omega t) \tag{4}$$

3. Influence of Actuator Parameters on Performance of Oscillating Systems

Normally, in order to simplify the analysis only the excitation force with K_E being constant irrespective of its variation versus displacements is considered, whilst the cogging force and reluctance force are both treated as zero. However, in the real working condition, all of them will introduce nonlinearities to the linear oscillating system and ultimately affect the system performance. Therefore, the influence of F_E, F_C and F_R on the oscillating system is investigated in this section.

3.1 Excitation Force

In some topologies of LOAs, e.g. SPM with small slot openings, the cogging force F_C can be negligible, whilst the reluctance force F_R can be regarded as zero due to negligible change of winding self-inductance. Hence, the thrust force produced by LOA is only comprised of F_E. As can be seen from (2b), F_E is largely dependent on the back-emf/force coefficient K_E, which is also a function of the displacement x. Therefore, the influence of F_E on the oscillation can be analyzed with regard to different K_E-x characteristics.

A. K_E=Constant

If K_E remains constant irrespective of the variation of displacements, the mechanical state-variable equation is:

$$K_E I_0 \sin(\omega t) - K_s x - D'_e v = m_e \frac{d^2 x}{dt^2} \tag{5}$$

where for simplification the pure damping load (F_L=$D_{el} v$) is considered; D_{el} and D'_e are the load and total equivalent viscous damping coefficients.

Due to the low-pass filter effect of the mechanical mass-spring-damper system, the steady-state displacement is essentially sinusoidal as:

$$x = A \sin(\omega t - \alpha) \tag{6}$$

where the oscillating amplitude A and the phase angle α between i and x are:

$$A = \frac{K_E I_0}{\sqrt{\left(K_s - m_e \omega^2\right)^2 + \left(D'_e \omega\right)^2}} \qquad \alpha = \tan^{-1} \frac{D'_e \omega}{K_s - m_e \omega^2}$$

whilst based on (5) and multiply it by the velocity gives:

$$P_{em} = \frac{1}{2} D_e \omega^2 A^2 + \frac{1}{2} D_{el} \omega^2 A^2 = P_{dl} + P_o \tag{7}$$

where P_{dl}, P_{em} and P_o are the system internal damping loss, electromagnetic and output powers. Neglecting the actuator iron loss, the system efficiency η_{sys} is given by:

$$\eta_{sys} = \frac{D_{el}\omega^2 A^2}{RI_0^2 + D'_e \omega^2 A^2} = \frac{D_{el}}{\frac{R}{K_E^2}\left[\left(\frac{K_s}{\omega} - m_e \omega\right)^2 + D_e'^2\right] + D'_e} \tag{8}$$

It is evident that η_{sys} achieves maximum (mechanical resonance) when:

$$\omega_n = \sqrt{\frac{K_s}{m_e}} \qquad x_n = -\frac{K_E I_0}{D'_e \omega_n}\cos(\omega_n t) \qquad P_{em\text{-}n} = \frac{K_E^2 I_0^2}{2D'_e}$$

B. K_E being a linear function of displacement

If the $K_E(x)$ characteristic exhibits profiles as shown in Fig. 1, the mechanical equation is:

$$K_E x I_0 \sin(\omega t) - K_s x - D'_e v = m_e \frac{d^2 x}{dt^2} \tag{9}$$

Assuming the steady-state solution having the same formation as (6) and neglecting harmonics, (9) becomes:

$$A(K_s - m_e \omega^2)\sin(\omega t - \alpha) + D'_e A\omega \cos(\omega t - \alpha) = \frac{1}{2} K_E A I_0 \cos(\alpha) \tag{10}$$

It is can be seen that A has to be zero so that (10) can be satisfied, meaning this case of K_E is incapable of producing stable sinusoidal oscillation.

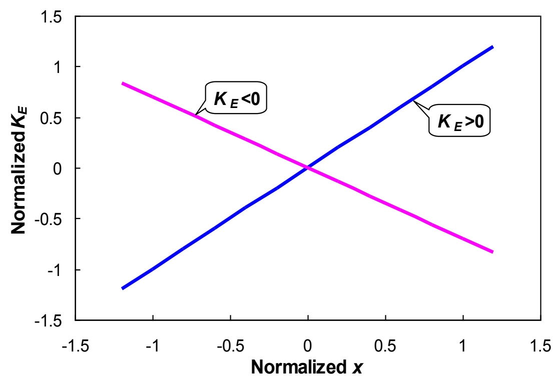

Fig. 1. Linear-slope $K_E(x)$ characteristics

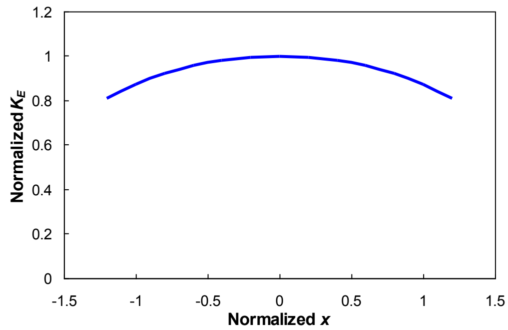

Fig. 2. Nonlinear $K_E(x)$ characteristics

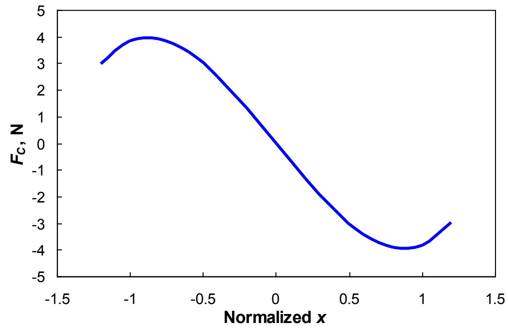

Fig. 3. An example of nonlinear $F_C(x)$ characteristic

C. Nonlinear K_E

As can be seen from Case *B*, in order to produce oscillation the K_E-x curve must not cross zero. However, the "roll-off" near the end of the rated stroke may exist in the K_E-x characteristic, making it look like the profile shown in Fig. 2. In this case, the characteristic can be curve-fitted over the rated stroke, and the K_E can be approximated as:

$$K_E(x) = K_{E0} - K_{E2}x^2 - K_{E4}x^4 - K_{E6}x^6 \cdots \tag{11}$$

where A_R is the rated stroke and $-A_R \le x \le A_R$.

For simplicity $K_E(x) = K_{E0} - K_{E2}x^2$ (K_{E0}, $K_{E2} > 0$) is used for analysis, and the mechanical equation becomes:

$$(K_{E0} - K_{E2}x^2)I_0 \sin(\omega t) - K_s x - D'_e v = m_e \frac{d^2 x}{dt^2} \tag{12}$$

Assuming the steady-state solution having the same formation as (6) and neglecting harmonics, (12) becomes:

$$A(K_s - \omega^2 m_e)\sin(\omega t - \alpha) + A\omega D'_e \cos(\omega t - \alpha) =$$

$$\left(K_{E0}I_0 - \frac{3K_{E2}I_0A^2}{4}\right)\cos(\alpha)\sin(\omega t - \alpha) + \left(K_{E0}I_0 - \frac{K_{E2}I_0A^2}{4}\right)\sin(\alpha)\cos(\omega t - \alpha) \tag{13}$$

Comparing the left and right sides of (13), A and α can be obtained by solving equation (14).

$$\begin{cases} A(K_s-\omega^2 m_e)=\left(K_{E0}I_0-\dfrac{3K_{E2}I_0A^2}{4}\right)\cos(\alpha) \\ A\omega D_e'=\left(K_{E0}I_0-\dfrac{K_{E2}I_0A^2}{4}\right)\sin(\alpha) \end{cases} \tag{14}$$

Due to the complication of (14), it is very difficult to derive a simple equation to determine the true resonant frequency. Alternatively, a quasi-resonant frequency can be regarded as:

$$\omega_{qn}=\sqrt{K_s/m_e}$$

while the mover displacement and electromagnetic power at the quasi-resonant condition are:

$$x=-A_{qn}\cos(\omega_{qn}t)$$

$$P_{em\text{-}qn}=\frac{1}{2}D_e'\omega_{qn}^2A_{qn}^2=\frac{1}{2D_e'}\left(K_{E0}I_0-\frac{K_{E2}I_0A_{qn}^2}{4}\right)^2$$

where $A_{qn}=2\dfrac{\sqrt{\omega_{qn}^2D_e'^2+K_{E0}K_{E2}I_0^2}-\omega_{qn}D_e'}{K_{E2}I_0}$.

It can be seen that compared to Case *A* with constant K_E, the nonlinear K_E has an adverse influence on the performance of the linear oscillating system, such as the reduction of oscillating amplitude, electromagnetic power and efficiency.

3.2 Cogging Force

In some LOA topologies with significant cogging force, the influence of cogging force on the oscillation has to be considered. In this part, its influence is investigated according to its distinctive gradient versus displacement, while the reluctance force F_R and the load force F_L are 0 and $D_{el}v$, respectively.

A. $F_C=k_c\cdot x$

If the F_C-x profile is represented by an ideal linear curve, the mechanical equation can be simplified as:

$$K_EI_0\sin(\omega t)-(K_s-k_c)x-D_e'v=m_e\frac{d^2x}{dt^2} \tag{15}$$

As can be seen, when $k_c>0$ the cogging force offsets the spring stiffness K_s, which is not recommended as the stiffness of the actual spring has to be increased in order to maintain the resonant operation at the supply frequency. However, if $k_c<0$ the cogging force enhances the spring stiffness, which, in other words, is conducive to reduce the stiffness of the actual spring to maintain the resonant oscillation at the supply frequency.

B. Nonlinear F_C

As can be seen from Case *A*, the F_C-x characteristic with negative gradient is more beneficial to the oscillation. However, the "roll-off" may be very common in the F_C-x characteristic, Fig. 3. In this regard, the characteristic can be curve-fitted over the effective stroke range as:

$$F_C(x)=-k_{c1}x+k_{c3}x^3+k_{c5}x^5+k_{c7}x^7\cdots \tag{16}$$

where $k_{c1}>0$ and $-A_R\le x\le A_R$.

In order to simplify the analysis, $F_C(x)=-k_{c1}+k_{c3}x^3$ (k_{c1}, $k_{c3}>0$) is used, and the mechanical equation can be re-written as:

$$K_EI_0\sin(\omega t)-K_s'x+k_{c3}x^3-D_e'v=m_e\frac{d^2x}{dt^2} \tag{17}$$

where $K'_s=K_s+k_{c1}$.

The steady-state solution to (17) can be assumed as (6), while neglecting other harmonics (17) becomes:

$$A\left(K_s'-m_e\omega^2-\frac{3k_{c3}A^2}{4}\right)\sin(\omega t-\alpha)+D_e'\omega A\cos(\omega t-\alpha)=K_EI_0\sin(\omega t) \tag{18}$$

Comparing the left and right sides, *A* and *α* can be obtained by solving (19):
The electromagnetic power is give by:

$$P_{em}=\frac{D_e'}{2}\frac{K_E^2I_0^2}{\left(\dfrac{K_s'-m_e\omega^2-\dfrac{3k_{c3}A^2}{4}}{\omega}\right)^2+D_e'^2}=\frac{1}{2}D_e'\omega^2A^2 \tag{20}$$

As can be seen, P_{em} will reach maximum when:

$$K_s'-m_e\omega^2-\frac{3k_{c3}A^2}{4}=0 \tag{21}$$

Thus, the resonant frequency ω_n and oscillating amplitude A_n are given by:

$$\begin{cases} D_e'\omega_nA_n=K_EI_0 \\ K_s'-m_e\omega_n^2-\dfrac{3k_{c3}A_n^2}{4}=0 \end{cases}$$

while α_n is 90°, the mover displacement and electromagnetic power are:

$$x=-A_n\cos(\omega_nt)$$

$$P_{em\text{-}n}=\frac{1}{2}D_e'\omega_n^2A_n^2=\frac{K_E^2I_0^2}{2D_e'}$$

In summary, this case with nonlinear F_C affects the resonant frequency and oscillating amplitude, whereas the phase angle between i and x, maximum electromagnetic power at resonance remain unchanged compared to that without F_C.

Furthermore, if the F_C-x characteristic is:

$$F_C(A_R) = -k_{c1}A_R + k_{c3}A_R^3 \le 0 \tag{22}$$

and $A_n \le A_R$, (21) becomes:

$$K_s' - m_e\omega_n^2 - \frac{3k_{c3}A_n^2}{4} \ge K_s' - m_e\omega_n^2 - \frac{3k_{c3}A_R^2}{4}$$

$$\Rightarrow K_s' - m_e\omega_n^2 - \frac{3k_{c3}A_n^2}{4} \ge K_s + \frac{k_{c1}}{4} - m_e\omega_n^2$$

Therefore, ω_n at resonance is:

$$\sqrt{\frac{K_s + \frac{k_{c1}}{4}}{m_e}} \le \omega_n < \sqrt{\frac{K_s'}{m_e}}$$

It can be seen that the cogging force with nonlinear F_C-x characteristic is still capable of enhancing the effective spring stiffness, although its contribution can be significantly compromised by k_{c3} compared to Case A with k_c<0.

4. Simulations

A tubular moving-magnet actuator based on [5], the schematic being shown in Fig.4, is utilized in this section as the test LOA for both state-variable modeling and numerical simulation.

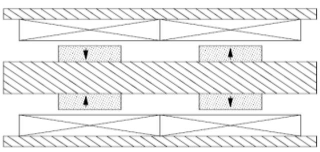

Fig.4. Schematic of a tubular moving-magnet actuator

Table 1. Main parameters of the actuator in Fig. 4

R, Ω	7	L, mH	5.0
K_E, N/A	4.2	m_e, kg	0.039
K_s, N/m	1884	D_e, s/m	3
A_R, mm	4		

4.1 Back-emf/force coefficient

Firstly, if the nonlinearity of back-emf/force coefficient is ignored, the main parameters of the actuator can be summarized in Table 2.1. Using Simulink, the LOA model is implemented as shown in Fig. 5, in which the current source is pre-set with fixed magnitude of 0.6 A and variable frequency. Fig. 6 shows the analytically calculated and simulated results of A, α, P_{em} and η on the test LOA, indicating the resonant frequency being ~35 Hz and the maximum efficiency being ~45%.

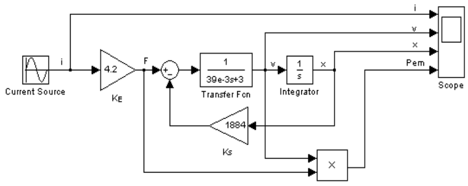

Fig. 5. Simulink block diagram for LOA system

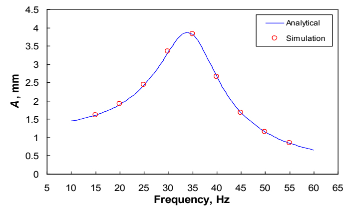

(a) Amplitude of oscillation

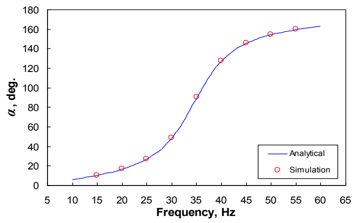

(b) i-x phase shift angle

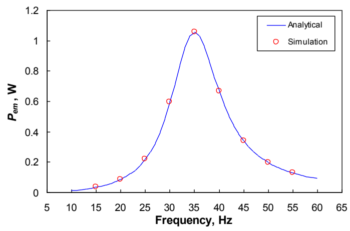

(c) Electromagnetic power

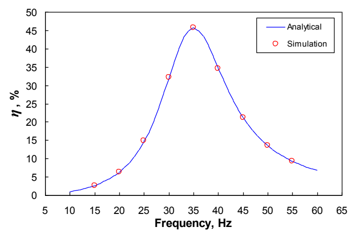

(d) Efficiency

Fig. 6. Comparison of analytical and simulated results

Secondly, to account for the nonlinearity of back-emf/force coefficient, the test LOA is used for the comparison of analytical and simulation results, whose main parameters are listed in Table 2. Fig. 7 shows the LOA model implemented in Simulink, in which the current source is pre-set with fixed magnitude of 0.6 A but variable frequency, whilst Fig. 8 compares the analytically predicted and simulated results of A, P_{em} and η on the test LOA, indicating the resonant frequency still remaining at ~35 Hz and the maximum efficiency being dropped to ~43.5% compared to the previous ~45% in the previous case, Fig. 9.

Table 2. Main parameters of the test actuator

R, Ω	7	L, mH	5.0
K_{E0}, N/A	4.2	K_{E2}, N/(Am$_2$)	52500
K_s, N/m	1884	m_e, kg	0.039
A_R, mm	4	D_e, s/m	3

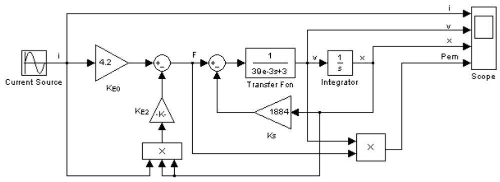

Fig. 7. Simulink block diagram for LOA system

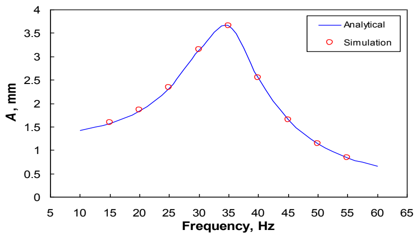

(a) Amplitude of oscillation

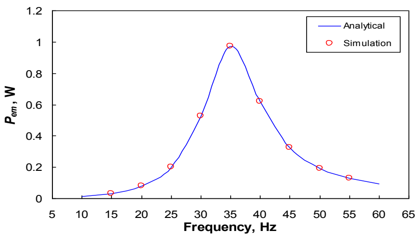

(b) Electromagnetic power

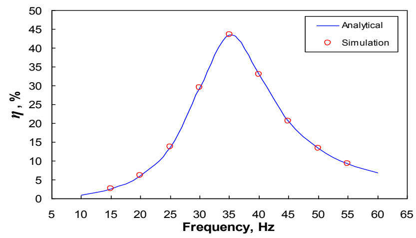

(c) Efficiency

Fig. 8. Comparison of analytical and simulated results

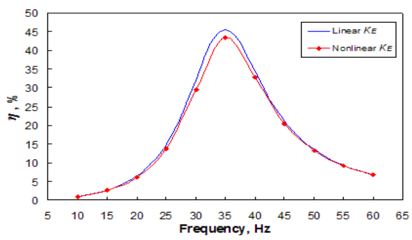

Fig. 9. Efficiency comparison of constant and nonlinear K_E

4.2 Cogging force

Table 3. Main parameters of the test actuator

R, Ω	7	L, mH	5.0
K_E, N/A	4.2	k_c, N/m	1750
A_R, mm	4	m_e, kg	0.039
K_s, N/m	1884	D_e, Ns/m	3

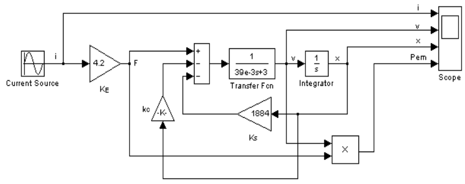

Fig. 10. Simulink block diagram for LOA system

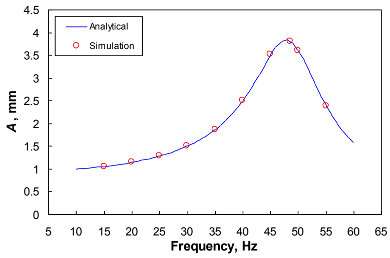

(a) Amplitude of oscillation

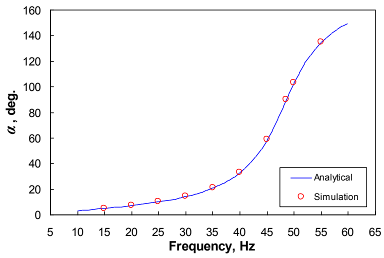

(b) i-x phase shift angle

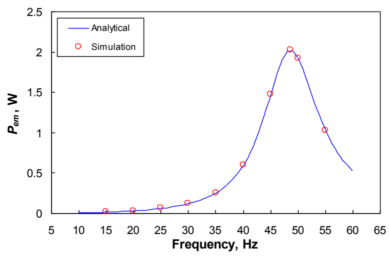

(c) Electromagnetic power

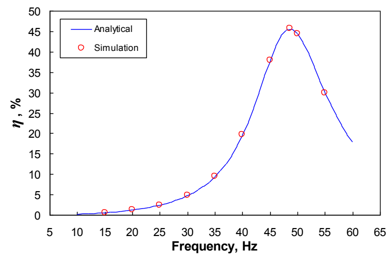

(d) Efficiency

Fig. 11. Comparison of analytical and simulated results

Firstly, the comparison of analytical and simulation results are undertaken based on the Simulink model shown in Fig. 10, in which the current source is pre-set with fixed magnitude of 0.83 A but variable frequency, while other major parameters are listed in Table 3. Fig. 11 is the comparisons of the analytically predicted and simulated results of A, α, P_{em} and η on the test LOA, showing the resonant frequency being shifted to ~48.6 Hz and the maximum efficiency remaining at ~45.6% the same as in Fig. 6.

Secondly, if nonlinear cogging force is considered, the simulation is undertaken based on the Simulink model shown in Fig. 12, in which the current source is pre-set with fixed magnitude of 0.83 A but with variable frequency, while other major parameters can be referred to as in Table 4. Fig. 13 compares the analytically predicted and simulated results of A, α, P_{em} and η on the test LOA. As can be seen, relatively good agreements are achieved between analytical and simulated results, while the discontinuity of responses, often referred to as the jump phenomenon, near resonance is observed in simulations. The predicted resonant frequency by analytical analyses is ~50.03 Hz with P_{em} and η being ~2.025 W and ~45.65%, respectively, whilst the resonant frequency by simulation is identified as ~50.6 Hz (relative difference<1.3%), but with essentially the same maximum P_{em} and η (being ~2.019 W and ~45.58% respectively) as the analytical data.

Table 4. Main parameters of the test actuator

R, Ω	7	L, mH	5.0
K_E, N/A	4.2	A_R, mm	4
k_{c1}, N/m	3859	k_{c3}, N/m^3	1.843×10^8
m_e, kg	0.039	D_e, Ns/m	3
K_s, N/m	1884		

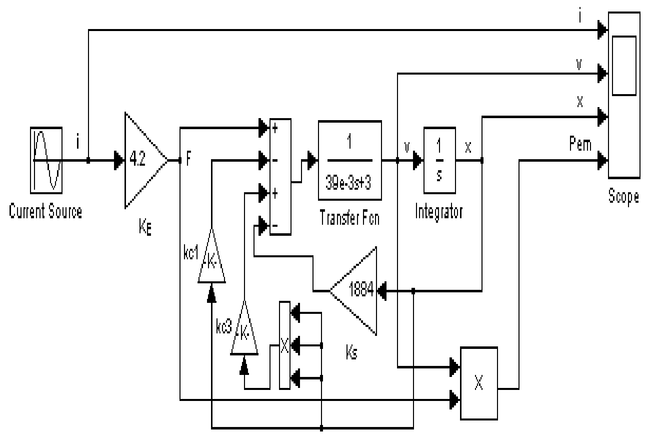

Fig. 12. Simulink block diagram for LOA system

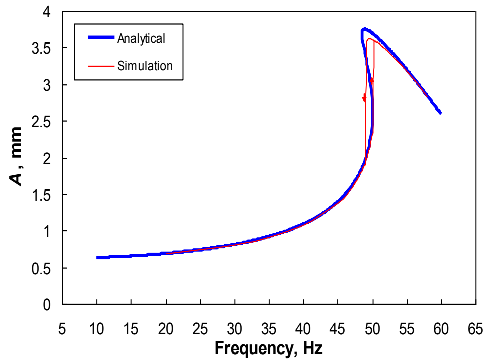

(a) Amplitude of oscillat ion

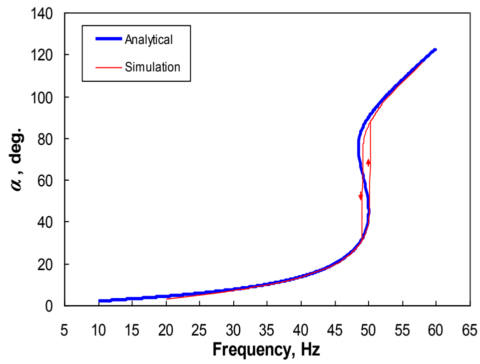

(b) *i*-*x* phase shift angle

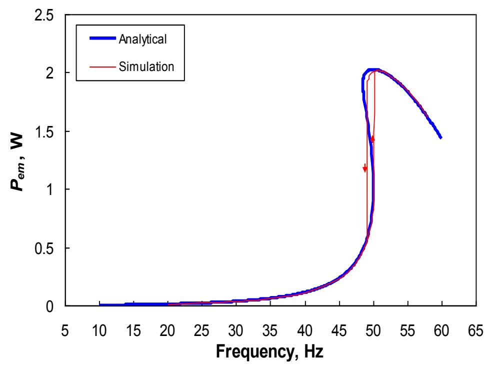

(c) Electromagnetic power

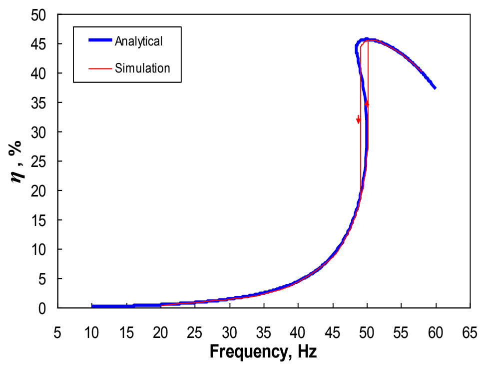

(d) Efficiency

Fig. 13. Comparison of analytical and simulated results

5. Conclusion

In this paper, both analytical and state-variable modeling techniques are used to investigate the influence of actuator parameters, such as back-emf/thrust force coefficient, cogging forces, on the performance of oscillating systems. Then the analytical derivations are validated by simulations, and good agreements are achieved. The conclusions of the paper potentially are capable of facilitating the design and evaluation of various PM linear actuators.

References

[1] T. W. Chun, J. R. Ahn, J. Y. Yoo and C. W. Lee, “Analysis and Control for Linear Compressor System Driven by PWM Inverter,” Proc. of the 30th annual conference of IEEE Industrial Electronics Society, pp. 263-267, Nov. 2004.

[2] S.M. Jang, J.Y. Choi, D.J. You, H.W. Cho, “The Influence of Mechanical Spring on the Dynamic Performance of a Moving-magnet Linear Actuator with Cylindrical Halbach Array,” in Proceedings of the 40th IEEE Industry Applications Society Annual Meeting (IAS’2005), pp. 2132-2139, Oct. 2005, Hong Kong, China.

[3] S. A. Evans, I.R. Smith, J.G. Kettleborough, “Permanent-magnet Linear Actuator for Static and Reciprocating Short-stroke Electromechanical Systems,” IEEE/ASME Transactions on Mechtronics, vol. 6, no. 1, pp. 36-42, Mar. 2001.

[4] L. N. Tutelea, M. C. Kim, M. Topor, et al, “Linear Permanent Magnet Oscillatory Machine: Comprehensive Modeling for Transients with Validation by Experiments,” IEEE Transactions on Industrial Electronics, vol. 55, no. 2, pp. 492-500, 2008.

[5] R.E. Clark, “Resonant Reciprocating Actuation Systems for Air-compressors,” Ph.D. Thesis, University of Sheffield, Jul. 1999.

[6] J. Wang, Z. Lin and D. Howe, “Characteristics of Linear Compressors under Current Source Excitation,” Proc. IMechE Part A: J. Power and Energy, vol. 221, pp. 1057-1065, 2007.

[7] R. E. Clark, G. W. Jewell and D. Howe, “Dynamic Modeling of Tubular Moving-magnet Linear Actuators,” Journal of Applied Physics, vol. 93, no. 19, pp. 8787-8789, 2003.

[8] B. Tomczuk, M. Sobol, “A Field-network Model of a Linear Oscillating Motor and its Dynamic Characteristics,” IEEE Transactions on Magnetics, vol. 41, no. 8, pp. 2362-2367, 2005.

[9] M. Utsuno, M. Takai, T. Mizuno, H. Yamada, “Comparison of the Losses of a moving-magnet Type Linear Oscillatory Actuator under Two Driving Methods,” IEEE Transactions on Magnetics, vol. 38, no. 5, pp. 3300-3303, Sep. 2002.

[10] G. S. Choe and K. J. Kim, “Analysis of Non-linear Dynamics in Linear Compressor,” JSME International Journal Series C, vol. 43, no. 3, pp. 545-552, 2000.

X. Chen received the B.Eng. and M.Eng. degrees from the College of Electrical Engineering, Zhejiang University, Hangzhou, China, in 2001 and 2004, respectively, and the PhD degree from the Department of Electronic and Electrical Engineering, University of Sheffield, UK, in 2012.

He is now working at Dyson, UK. His research interest is linear and rotary permanent magnet machines and control.

Z. Q. Zhu received the B.Eng. and M.Sc. degrees in electrical and electronic engineering from Zhejiang University, Hangzhou, China, in 1982 and 1984, respectively, and the Ph.D. degree in electrical and electronic engineering from the University of Sheffield, Sheffield, U.K., in 1991.

Since 1988, he has been with the University of Sheffield, where he is currently a Professor at the Department of Electronic and Electrical Engineering, Head of the Electrical Machines and Drives Research Group, Academic Director of Sheffield Siemens Wind Power Research Centre. His current major research interests include design and control of permanent magnet brushless machines and drives, for applications ranging from automotive to renewable energy. He is a Fellow of IEEE.